ChemPubSoc Europe

DOI: 10.1002/open.201800020

Open Access ChemistryOPEN Full Papers

Synthesis and Characterization of Novel Fluoro-glycosylated Porphyrins that can be Utilized as Theranostic Agents

Katriann Arja[+],[a] Mathias Elgland[+],[a] Hanna Appelqvist,[a] Peter Konradsson,[a] Mikael Lindgren,[b] and K. Peter R. Nilsson*[a]

Small molecules with modalities for a variety of imaging techniques as well as therapeutic activity are essential, as such molecules render opportunities to simultaneously conduct diagnosis and targeted therapy, so called theranostics. In this regard, glycoporphyrins have proven useful as theranostic agents towards cancer, as well as noncancerous conditions. Herein, the synthesis and characterization of heterobifunctional glycoconjugated porphyrins with two different sugar moieties, a common monosaccharide at three sites, and a 2-fluoro-2-deoxy glucose (FDG) moiety at the fourth site are presented. The fluoro-glycoconjugated porphyrins exhibit properties for multimodal imaging and photodynamic therapy, as well as specificity towards cancer cells. We foresee that our findings might aid in the chemical design of heterobifunctional glycoconjugated porphyrins that could be utilized as theranostic agents.

1. Introduction

With the recent progress in chemical biology and medicinal imaging, opportunities to simultaneously conduct diagnosis and targeted therapy, so called theranostics, have evolved.[1] In this regard, the development of small-molecule-based multimodal theranostic agents, having modalities for a variety of imaging techniques as well as therapeutic activity, are essential. From an imaging perspective, magnetic resonance imaging (MRI) and positron emission tomography (PET) can be used in organ to the full-body scale, whereas resolution at the cellular and molecular level is obtained using optical imaging, such as two-photon microscopy and super-resolved fluorescent imaging. In addition, a therapeutic effect can be achieved by a variety of chemical modifications, such as conjugation of drugs or photosensitizers, to the theranostic agents.

[a] K. Arja,[+] M. Elgland,[+] Dr. H. Appelqvist, Prof. P. Konradsson, Prof. K. P. R. Nilsson
Division of Chemistry
Department of Physics, Chemistry and Biology
Linköping University
581 83 Linköping (Sweden)
E-mail: petni@ifm.liu.se

[b] Prof. M. Lindgren
Department of Physics
Norwegian University of Science and Technology, NTNU
7491 Trondheim (Norway)

[+] These authors contributed equally to this work

Supporting Information and the ORCID identification number(s) for the author(s) of this article can be found under: https://doi.org/10.1002/open.201800020.

Porphyrins are a fascinating class of molecules that display remarkable photophysical properties that can be utilized for both optical imaging and photodynamic therapy (PDT), a minimally invasive therapy that combines a photosensitizer (PS) and radiation with light of a specific wavelength to initiate toxic radical reactions. A variety of porphyrin derivatives have been evaluated as theranostic agents towards cancer, as well as noncancerous conditions, including infectious diseases.[2–4] However, developing porphyrin-based PDT agents with multifunctional imaging capabilities and improved pharmacokinetic and pharmacodynamic characteristics, such as tumor specificity and solubility, remains a challenge. In this regard, glycoporphyrins have evolved as an interesting class of theranostic agents, as the addition of carbohydrates to the porphyrin scaffold has shown an impact on the biological behavior of these compounds, both in terms of cellular uptake and subcellular localization, as well as specificity towards cancer cells.[5–13] For instance, it is well known that cancer cells display increased glucose uptake and metabolism, a phenomenon known as the Warburg effect, through the glucose transporter (GLUT) proteins and that other carbohydrate motifs can also be taken up by the cell through these transporters.[14–16] Hence, glycoporphyrins can be designed to specifically target cancer cells.

Besides enhanced cellular uptake, molecules that are to act as photosensitizers in PDT must remain in target tissue for a reasonably long time in order to elicit a therapeutic effect. This necessitates an adequate metabolic stability and trapping of the theranostic agents in cancer cells. In this regard, 2-fluoro-2-deoxy glucose (FDG) is a glucose derivative, where the hydroxyl group at the second carbon has been replaced by a fluorine and, owing to the absence of the C2-hydroxyl, FDG cannot be metabolized in the same manner as glucose and is thereby trapped in the cell.[17,18] 2-[18F]Fluoro-2-deoxy glucose

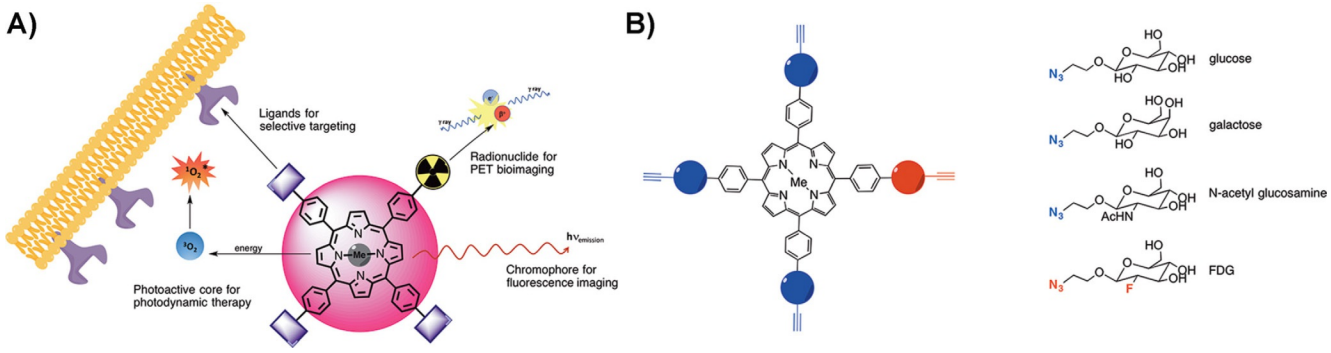

Figure 1. A) Schematic drawing showing desirable properties of a porphyrin-based theranostic agent. B) A porphyrin scaffold featuring two different alkyne-functionalized handles (blue and red) for consecutive click-reactions (left). The 2-azidoethyl β-D-glycosides that was conjugated to the blue and red sites, respectively, on the porphyrin scaffold (right).

([18F]FDG) is also, by far, the most widely employed radiotracer and is routinely used for PET imaging at clinics in both oncology and neurology.[19–21] Hence, conjugation of this glucose derivative to porphyrins might render dual modes, metabolic trapping, and PET imaging to porphyrin-based theranostic agents.

An optimal glycoporphyrin-based theranostic agent should preferably exhibit properties for multimodal imaging and PDT, as well as specificity towards distinct molecular targets (Figure 1 A). In addition, the synthetic methodology to render the desired carbohydrate-functionalized porphyrins must be robust and allow for late-stage conjugation of the sugar modalities, so as to avoid multiple linear synthetic routes. Literature reports on the synthesis of glycosylated porphyrins include both porphyrin formation from the acid-catalyzed condensation of sugar-functionalized aldehydes with pyrrole and a coupling reaction between sugar units and an already mature porphyrin.[6,8,22] Herein, we present synthetic routes that can be utilized to achieve heterobifunctional glycoconjugated porphyrins with two different sugar moieties, a common monosaccharide (glucose, galactose or *N*-acetyl glucosamine) at three sites, and an FDG moiety at the fourth site (Figure 1 B). As azide alkyne Huisgen cycloaddition,[23,24] whereby molecular moieties can be added together by using a copper(I) catalyst at room temperature, has been used by several groups to link carbohydrates to tetrapyrrolic species,[22,25] the heterobifunctional porphyrinic starting material holds two types of singly addressable terminal attachment points that can be functionalized with desired azide-functionalized carbohydrate moieties (Figure 1 B). From a photophysical perspective, the glycoporphyrins were demonstrated to display fluorescent properties for optical imaging as well as the generation of singlet oxygen. In addition, properly functionalized glycoporphyrins showed selectivity towards malign melanoma cells. We foresee that these FDG-conjugated glycoporphyrins can be evaluated as theranostic agents towards cancer and infectious diseases.

2. Results and Discussion

2.1. Synthesis of an Asymmetric Porphyrin Moiety and Azido Sugars

To selectively couple two different carbohydrates sequentially to the porphyrin, it must be equipped with orthogonal functional groups. Synthesis of asymmetrical porphyrins with an appropriate substitution pattern can be afforded by a demanding rational approach with step-by-step synthesis, leading to di- or tri-pyrrolic intermediates that eventually form the desired porphyrin in low-yielding condensation reactions.[26] However, this approach was not feasible in our study, because an easily accessible starting porphyrin was desired as a further multistep synthesis was to be done to reach the target compounds. From this perspective, methyl mono-(*p*-carboxy)tetraphenylporphyrin (Me-pcTPP) **8** was chosen as the starting porphyrin, and this molecular entity was obtained through Lindsey's method in an one-pot, two-step reaction between pyrrole, benzaldehyde, and methyl 4-formylbensoate under the $BF_3{\cdot}OEt_2$ catalysis followed by 2,3-dichloro-5,6-dicyanobenzoquinone (DDQ) oxidation.[26] Despite the stoichiometric molar ratios of pyrrole and the aldehydes, the reaction gives an expectedly poor yield of the target porphyrin. However, a slight modification of the reaction conditions by adding NaCl to a final concentration of 0.1 M effectively doubled the isolated yield from 8 to 19%. A similar effect has previously been observed by Lindsey and co-workers.[27]

Porphyrin **8** was further modified to install appropriate coupling modalities (Scheme 1). Treatment with chlorosulfonic acid easily yielded chlorosulfonated porphyrin **9**, which was immediately reacted with propargylamine in the presence of *N*,*N*-diisopropylethylamine (DIPEA) to yield a tris-alkyne functionalized porphyrin with one ester site (compound **10**). To avoid the insertion of copper into the porphyrin cavity during the upcoming click reactions, metalation with zinc by using $Zn(OAc)_2{\cdot}2H_2O$ was performed on the tris-alkynylated porphyrin to produce compound **11** in 40% yield over three steps. Prior to coupling to the carbohydrates through the click reac-

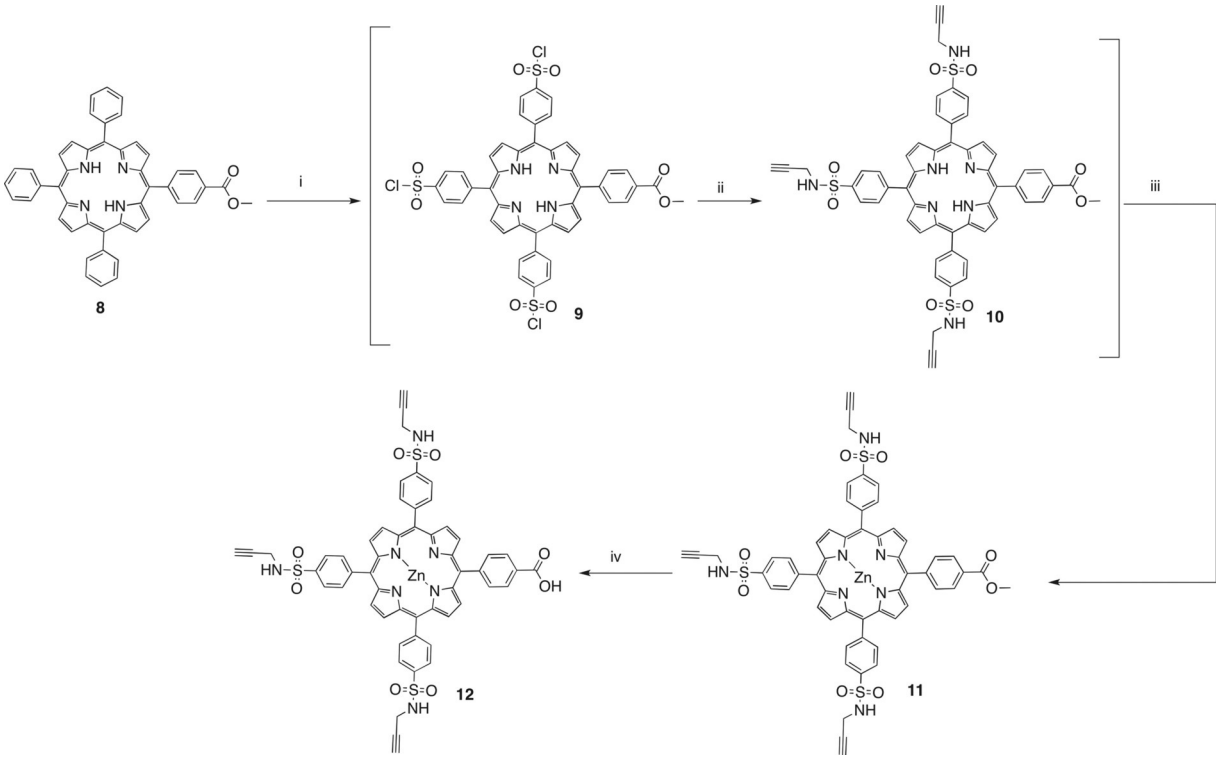

Scheme 1. General conditions and reagents: i) HSO_3Cl, room temperature; ii) propargylamine, DIPEA, DCM, room temperature; iii) $Zn(OAc)_2 \cdot 2H_2O$, DCM, MeOH, room temperature, 40% over three steps; iv) LiCl, DMF, MW, 160 °C, 77%.

tion, the methyl ester on the porphyrin had to be hydrolyzed to the corresponding acid for later reaction. Conventional basic ester hydrolysis with a minimal excess of sodium hydroxide in a tetrahydrofuran (THF)–water mixture unfortunately gave partial hydrolysis of the sulfonamide bonds. Therefore, the Krapcho demethylation was employed, using lithium chloride in dimethylformamide (DMF) under microwave irradiation,[28–30] successfully providing compound **12** in 77% yield without any indication of side reactions.

Non-fluorinated azidosugars were synthesized according to known synthetic procedures (Scheme S1).[31–33] 2-Azidoethyl β-D-glycosides **4** and **5** were synthesized according to a literature procedure reported by Chernyak et al.,[31] starting from per-acetylated D-glucose and D-galactose, respectively, that were subjected to a boron-trifluoride diethyerate-promoted glycosylation to 2-chloroethanol followed by an azidation using NaN_3 and tetra-*n*-butylammonium bromide (TBAB) in DMF at 80 °C. Azide-equipped *N*-acetyl glucosamine **6** was synthesized, starting from per-acetylated D-glucosamine that was converted to its corresponding oxazoline by using the method described by Nakabayashi et al.[32] followed by a pyridinium *p*-toluene sulfonate (PPTS)-promoted glycosylation to 2-chloroethanol,[33] and finally, azidation using NaN_3 and TBAB in DMF at 80 °C. The synthesis of β-configured clickable FDG **7** followed the newly published methodology according to Elgland et al.[34] All of the azidosugars were achieved in adequate yields.

2.2. Synthesis of Heterobifunctional Glycoporphyrins

Compound **12** was reacted with **4**, **5**, or **6** through Sharpless' copper(I)-catalyzed modification of the Huisgen 1,3-cycloaddition[23] under microwave activation to yield **13**, **14** and **15**, respectively (Scheme 2). The microwave protocol, adapted from Maillard and co-workers,[35] was mild and highly efficient, requiring only 5 min reaction time at 85 °C in a sealed vial under microwave irradiation. LC–MS analysis of the crude reaction mixture revealed complete conversion of the starting material into product for the all three reactions, and isolated yields ranged between 59 and 89%. NMR analysis along with MS data confirmed the identity of the triglycosylated porphyrins, where the triazole protons give rise to a characteristic singlet at around 8 ppm in the ^{1}H NMR spectra.

Owing to the simplicity and effectiveness of the microwave-assisted click reaction, this method was also selected for the final fluoro-glycosylation of conjugates **13**, **14**, and **15**. Therefore, the free acid at **13**, **14**, and **15** underwent 1-ethyl-3-(3-dimethylaminopropyl)-carbodiimide/N-hydroxysuccinimide (EDC/NHS)-facilitated amide coupling reactions to propargyl amine, providing corresponding alkynes **16**, **17**, and **18**. The procedure for click conjugation of **16**, **17**, and **18** to FDG **7** was performed as described above. However, the reaction times had to be prolonged, most likely because of the reduced reactivity of the fluorine substituted glycosyl azide as compared to its non-fluorinated counterparts. The successful fluoro-glycosylation was evident in LC–MS analysis as well as in NMR data, with the ^{1}H NMR indicating two different triazole signals at

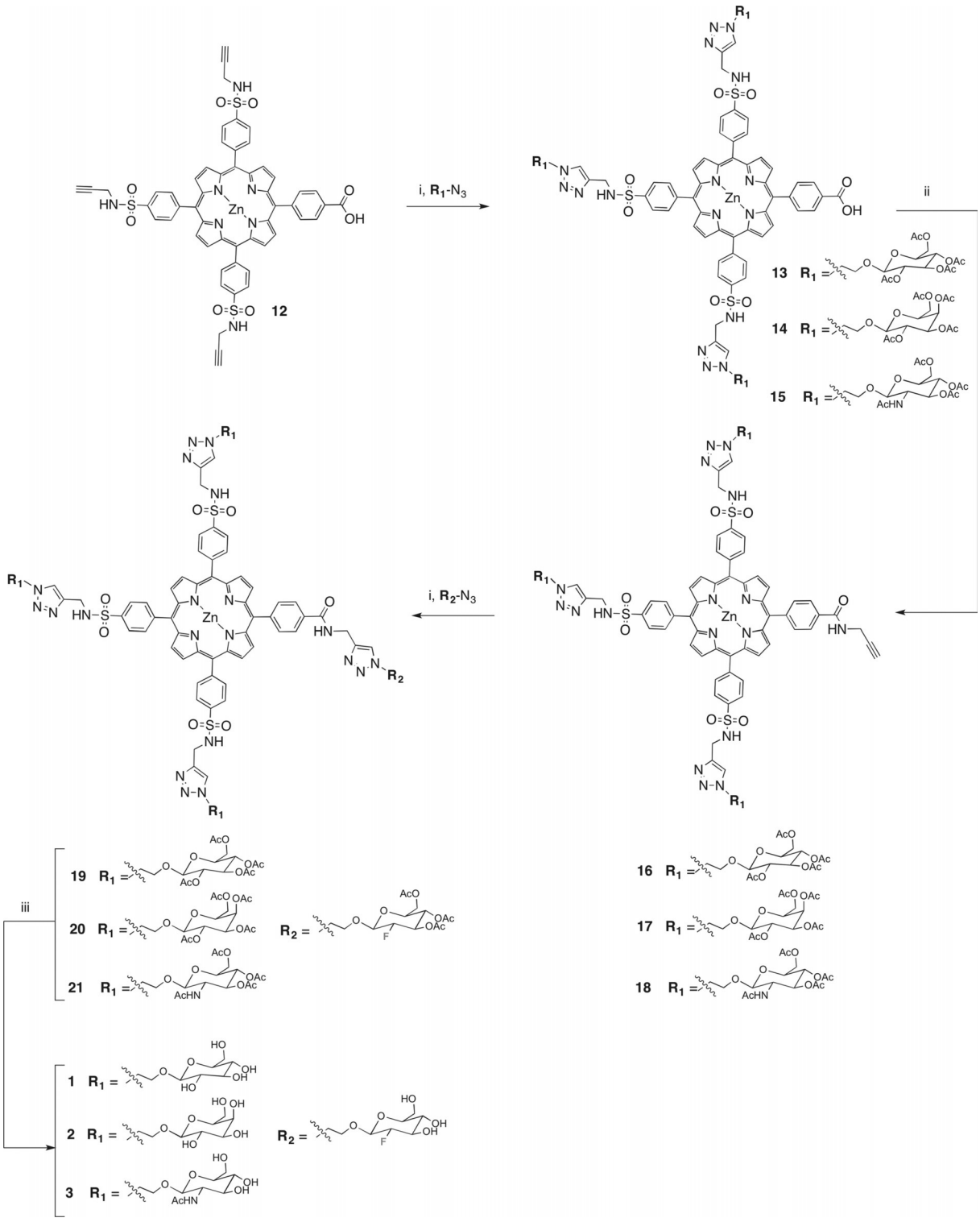

Scheme 2. General conditions and reagents: i) $CuSO_4$, sodium L-(+)-ascorbate, THF, *t*-BuOH, H_2O, MW, 85 °C, 59% (**13**), 89% (**14**), 84% (**15**), 62% (**19**), 55% (**20**), 78% (**21**); ii) 1. NHS, EDC, DMF, room temperature; 2-propargylamine, DIPEA, room temperature, 85% (**16**), 61% (**17**), 52% (**18**); iii) NaOH, MeOH, H_2O, room temperature, 99% (**1**), 80% (**2**), quant. (**3**).

around 8 ppm and ^{19}F NMR giving rise to a characteristic doublet of doublets at −199 ppm. Fully glycosylated compounds **19**, **20**, and **21** were subsequently deacetylated, yielding target molecules **1**, **2**, and **3**, respectively, in very good yields.

Compounds **23** and **24** (Figure S1) were synthesized to be used as reference substances for the cell studies in conjunction to the synthetic work in question. To probe the potential metabolic trapping effect of the fluoro-glycosylated porphyrins, the tetra-glucosylated porphyrin **23** was synthesized. Compound

23 was produced from triglycosylated alkynyl porphyrin **16** by applying the synthetic steps illustrated in Scheme 2, with the alteration of using azidoethyl β-glucoside **4** instead of FDG **7** in the second glycosylating click reaction. Non-glycosylated tetrasulfonated porphyrin **24** was synthesized from the corresponding unmetalated porphyrin through the previously used procedure (vide supra) in order to assess the effect of the sugar units in terms of cellular uptake.

2.3. Photophysical Characterization of the Glycoporphyrins

The fluoro-glycosylated porphyrins **1**, **2** and **3**, dissolved in DMSO and further diluted in phosphate buffered saline pH 7.4 (PBS), showed distinct absorption bands around 430, 565, and 605 nm, respectively, and these bands can be assigned to the typical Soret band and Q bands of the porphyrin moiety (Figure 2). In addition, upon excitation at 430 nm, two distinct emission peaks around 615 and 665 nm were observed in the emission spectrum for all fluoro-glycosylated porphyrins and similar emission spectra were observed when using excitation at 565 nm (Figure 2). Reference compounds **23** and **24** displayed similar photophysical characteristics to the fluoro-glycosylated porphyrins (Figure S1).

To evaluate the photo-oxidizing capability of the fluoro-glycosylated porphyrins, a proto-variant of glucosylated FDG–porphyrin conjugate lacking the Zn^{2+} (compound **1′**, Figure S1) was prepared. Compound **1′** was produced by demetalation of **19** with trifluoroacetic acid followed by deacetylation of the sugar units with aqueous sodium hydroxide. The absorption spectra of **1′** showed the characteristic features of a proto-porphyrin with the strong Soret absorption band at 419 nm, and the weaker Q bands at 515, 549, 590, and 646 nm (Figure 3A). The latter are a consequence of the lowered symmetry of the porphyrin ring (as compared to the Zn analogues) induced by the pair of N–H bonds that splits the Q band into two components: one along the N–H axis of the planar ring structure, the other perpendicular to the N–H bond, still within the plane of the ring. This ring symmetry splitting is further split by vibrational substructures and four distinct bands are generally observed.[36] In agreement with earlier studies of proto-porphyrins,[37] excitation in the Soret band resulted in fluorescence emission peaks at 655 and 720 nm (Figure 3B) with a decay time of 10.4 ns (data not shown), as measured by using the time-correlated single-photon-counting method.

To confirm the generation of singlet oxygen by using the photosensitizer, the triplet excited-state absorption was recorded for UV excitation ($\lambda = 355$ nm, Figure 3C). Here, the solvent had been flushed with argon to remove oxygen, as it is known to strongly quench the triplet state. In the pump-and-probe experiment, the laser is first exciting the singlet-state levels and, via intersystem, a fraction converts into the triplet state. Synchronously with the excitation pulse, a white flash lamp is triggered and used to measure the light transmitted through the excited sample by using an array detector that simultaneously measures the whole spectrum. By recording various reference signals (with/without laser flash; with/without white flash), the transient absorption can be calculated as the ratio between the pumped and unpumped absorption signal (for details on the analysis and procedure, see Glimsdal et al.[38]). As shown in Figure 3C, the ground-state absorption will appear

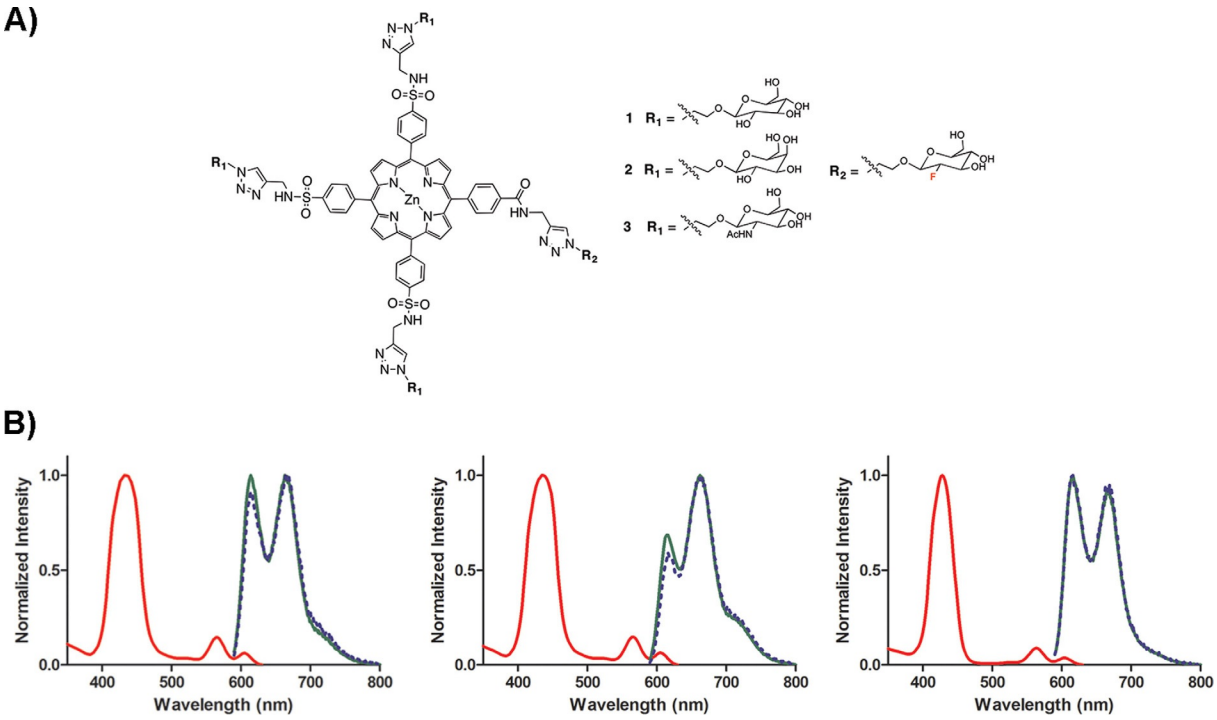

Figure 2. A) Chemical structure of fluoro-glycosylated porphyrins **1**, **2**, and **3**. B) Photophysical characteristics of fluoro-glycosylated porphyrins **1** (left), **2** (middle), and **3** (right). Absorption spectra are shown as red solid lines, whereas emission spectra are shown as green solid lines (excitation at 430 nm) or blue dotted lines (excitation at 561 nm). The fluoro-glycosylated porphyrins were dissolved in DMSO to a concentration of 1.5 mM and further diluted in PBS to a final concentration of 15 μM prior to measurements.

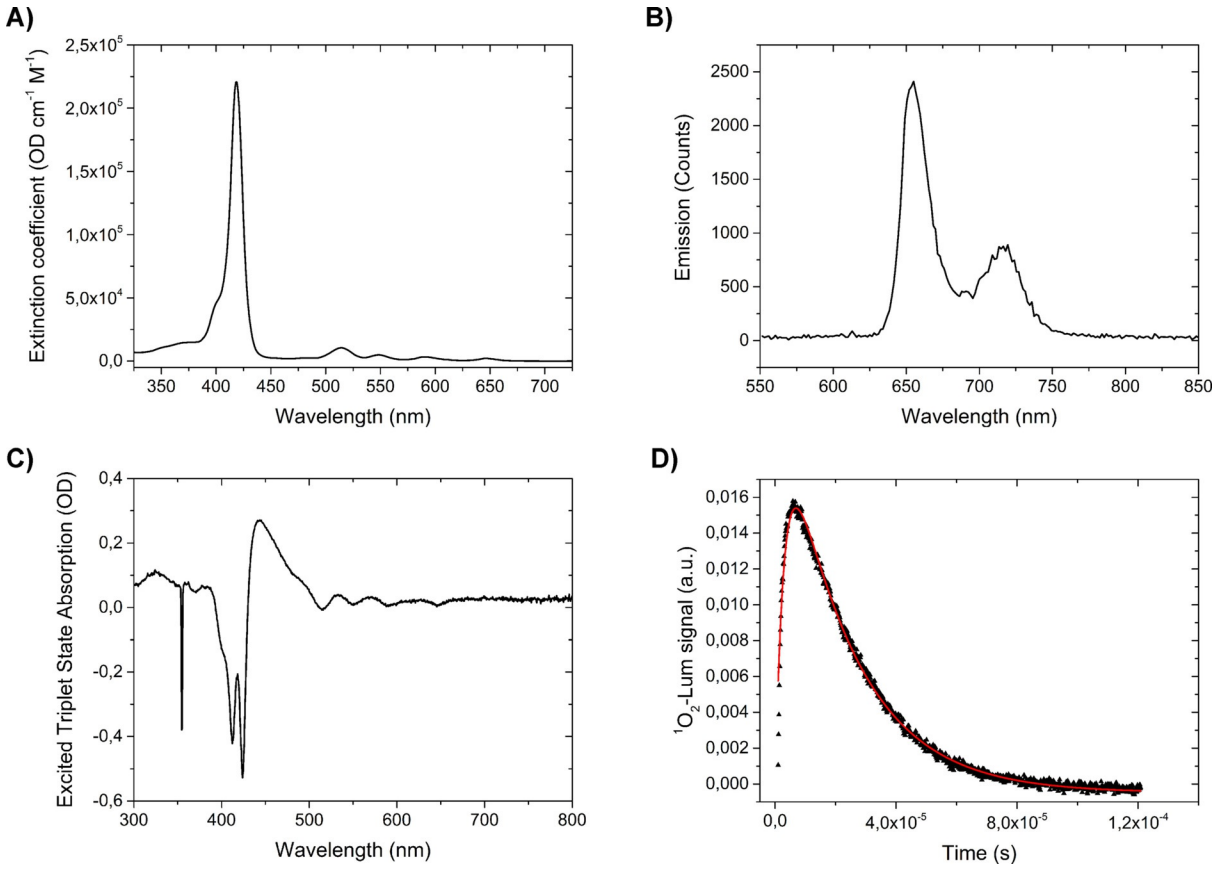

Figure 3. Photophysical characterization of **1′**: A) Absorption spectrum; B) emission spectrum (excitation at 419 nm); C) triplet excited-state absorption spectrum (excitation at 355 nm); D) transient luminescence at 1270 nm of singlet oxygen generated by **1′** (excitation at 440 nm). For all the measurements, THF was used as solvent and argon gas was used to remove oxygen from the solvent.

with negative phase and contains the same information as the absorption spectrum (Figure 3 A). The triplet absorption appears in positive phase, notably around 450 nm (strong) and 325 nm (weaker). One can also see the distinct spike at 355 nm, originating from the excitation pulse as it overlaps with the gated detection at zero delay, where the triplet absorption is largest.

The formation of singlet oxygen of compound **1′** was also verified with a transient luminescence measurement that was carried out by using a nanosecond-pulsed tunable OPO laser as the excitation source with a wavelength of 440 nm (being in the tail of the Soret band of **1′**). Solutions of **1′** in THF were prepared, with the concentration corresponding to an absorbance of approximately optical density (OD) 0.15 at the excitation wavelength. The luminescence at 1270 nm was selected by using optical filters and recorded in a 90° configuration by using a photomultiplier tube (PMT) and a transient recorder (Figure 4 D). Samples were exposed to air prior to the measurements. A typical measured transient is shown in Figure 4 D. Following Snyder et al.,[39] the transient line shape can be fitted to the following expression [Eq. (1)]:

$$\left[O_2\left(a^1\Delta_g\right)\right]_t = \frac{k_{form}}{k_\Delta - k_T}\left[O_2\left(X^3\Sigma_g^-\right)\right]\cdot[T]_0\left(e^{-k_T t} - e^{-k_\Delta t}\right) \quad (1)$$

where the time-dependence signal is determined by three rates k_T, k_Δ, and k_{form}, (decay of the porphyrin triplet, decay of singlet oxygen and rate of singlet oxygen generation, respectively), as well as the concentration of ground state triplet state oxygen in the solvent $[O_2(X^3\sum_g^-]$, and the concentration of triplets $[T]_0$ at time = 0. The former two rates can be uniquely defined from the shape of the signal, whereas k_{form} and the concentrations will be contained in a single pre-exponential factor. Thus, the rates could be fitted to calculate the corresponding life-times ($\tau = 1/k$) for the triplet and singlet oxygen lifetimes to $\tau_T = 2.97$ +/-0.02 µs and $\tau_\Delta = 22.3$ +/-0.08 µs, with the pre-exponential factor being 0.018. These lifetimes are typical for proto-porphyrin, and as a comparison the lifetime of singlet oxygen is only a few microseconds in water, and nearly 70 µs in D_2O.[39,40]

2.4. Biological Characterization of the Glycoporphyrins

To investigate the behavior of the glycoporphyrins in a biological system, we next tested the compounds in cell culture models, both normal human fibroblasts and a melanoma cell line. The porphyrin variants were added to complete cell culture medium for 24 h and cells were, thereafter, fixated and investigated by microscopical examination. As seen in Figure 4, there was a drastic difference in the staining of the different

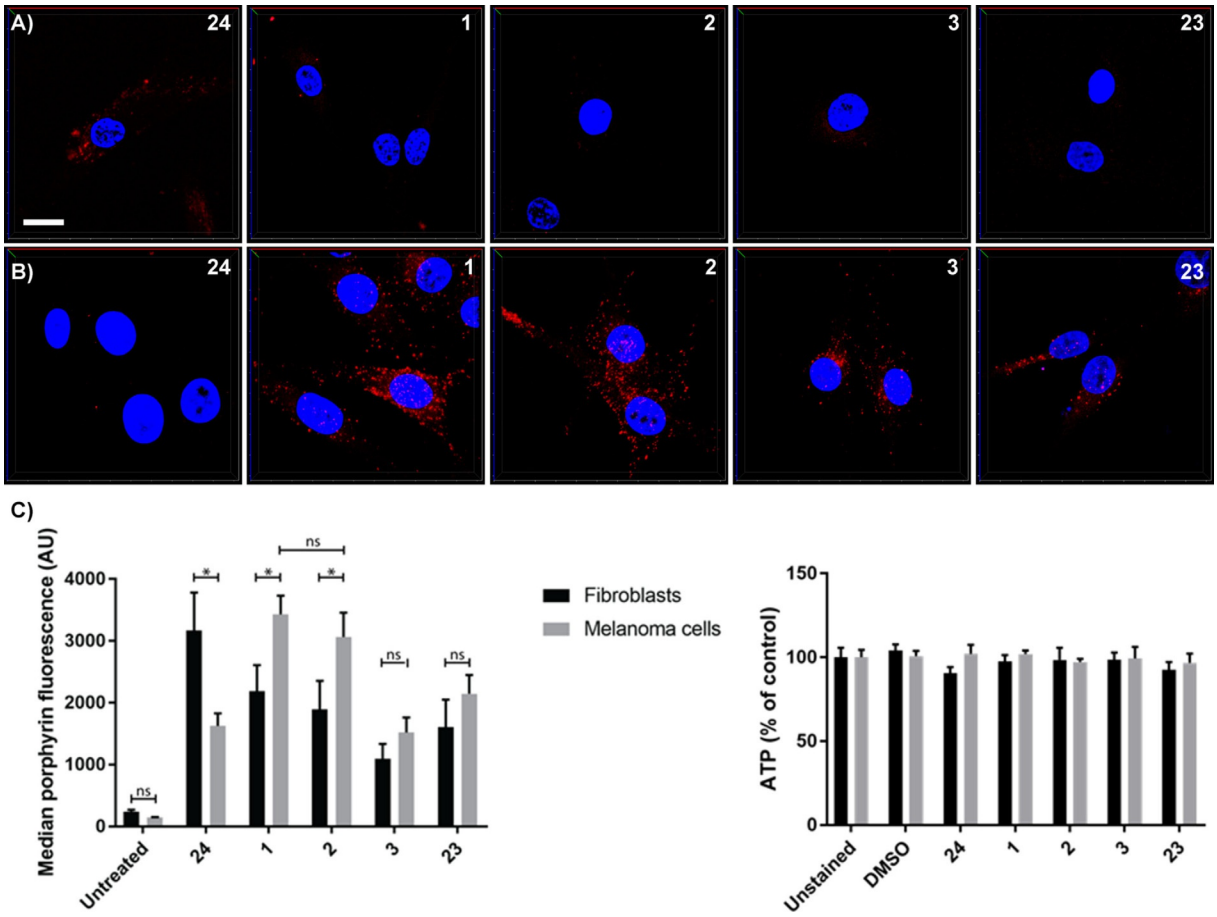

Figure 4. Confocal microscopy 3D images of A) fibroblasts and B) melanoma cells stained with porphyrins (red) and DAPI (nuclei staining; seen in blue). The cells were incubated with the porphyrin variants (20 μM, 24 h) and, thereafter, fixated. Images were collected in *z*-stack spectral mode (excitation at 405 and 561 nm) with the dimensions $x = 135$ μm, $y = 135$ μm and $z = 20$ μm. Scale bar 20 μm. C) Flow cytometry analysis of cells exposed to porphyrin variants (20 μM, 24 h) in complete cell culture medium. Fluorescence intensities are compared in fibroblasts and melanoma cells stained with unglycosylated **24**, FDG glycoporphyrins **1**, **2**, and **3**, and non-fluorinated glucoporphyrin **23**. Diagram shows the combined results of four replicate measurements. Significant differences were determined by ANOVA and $p \leq 0.05$ are indicated with asterisks. D) Cell viability, determined by ATP content, in cell cultures exposed to porphyrin variants (20 μM, 24 h). Data is presented as mean + SD ($n = 4$). Statistical evaluation using ANOVA demonstrate no significant alterations in cell viability compared to unstained controls. Final concentration of DMSO added to cells was 0.13%.

variants and in malignant cells compared to normal cells. In fibroblasts, the unglycosylated porphyrin, **24**, displayed rather intense staining, observed as a punctate perinuclear staining pattern, whereas only minor staining was observed for the glycosylated porphyrins **1**, **2**, **3**, and **23** (Figure 4A). In contrast, superior punctate perinuclear staining patterns were seen with **1** and **2** in melanoma cells (Figure 4B). Compounds **3** and **23** showed slightly less efficient staining in melanoma cells, whereas no observable staining was obtained with the unglycosylated porphyrin, **24**. (Figure 4B). Together, these results verified that the glycosylation of the porphyrin is a chemical determinant for achieving selectivity towards cancer cells. Furthermore, in line with previous reports,[5,7,8] porphyrins with galactose (**2**) and glucose (**1**) modalities displayed an enhanced uptake in cancer cells compared to the *N*-acetyl-glucosamine-functionalized porphyrin, **3**. The observed difference in staining between glycoporphyrin **1** and **23** also indicated that the FDG moiety might render a metabolic trapping of the photosensitizer.

To obtain quantitative data, the porphyrin fluorescence intensity in cells was analyzed by flow cytometry. After exposure to 20 μM of the respective porphyrin derivatives for 24 h, cells were detached and the fluorescence intensity of individual cells was registered. As shown in Figure 4C, the flow cytometry data confirmed the microscopy results. The highest staining intensity in melanoma cells was achieved by using compounds **1** and **2** (Figure 4C), demonstrating a superior effect of the addition of glucose or galactose. *N*-Acetyl glucosamine FDG porphyrin **3** showed a lower staining intensity and no significant difference in uptake between fibroblasts and melanoma cells. The non-glycosylated porphyrin **24** displayed a preferential uptake into fibroblasts compared to melanoma cells, confirming the necessity of glycosylation of porphyrins in order to have potential as tumor-selective PDT agents. The fluorinated glucose analogue **1** displayed a significant preferential uptake into melanoma cells compared to the non-fluorinated glucosylated porphyrin **23**, indicating that the conjugation of FDG has an obvious positive effect on trapping the theranostic agents

in cancer cells. However, more experiments are required to unveil this effect in more detail.

To identify the intracellular location of porphyrin **1**, co-staining experiments with a variety of organelle markers, including mitotracker, LAMP2, Golga, calnexin, Eea1, and PMP70 were performed for compound **1**-stained malignant melanoma cells. However, these experiments were not successful, as the porphyrin staining was misrepresented after using the permeabilization buffer for achieving consistent antibody staining. The permeabilization buffers tested contained Triton X (0.1%) or saponin (0.1%) and the porphyrin staining pattern was not evident after treating the cells with permeabilization buffers, suggesting that compound **1** staining in melanoma cells was sensitive to detergents.

Finally, as photosensitizers optimally are non-toxic in the absence of light exposure, the toxicity of the compounds in both normal human fibroblasts and a melanoma cell line were evaluated. The viability of cell cultures after porphyrin exposure was determined by quantitatively measuring the ATP content of the cells, and none of the tested compounds induced any significant decrease in viability compared to unexposed controls (Figure 4C). In addition, no alterations in cell morphology, indicating toxic effects, were observed (data not shown).

3. Conclusions

Synthetic routes for achieving FDG-functionalized heterobifunctional glycoporphyrins have been established. The FDG glycoporphyrins exhibit fluorescent properties for optical imaging as well as the generation of singlet oxygen. In addition, properly functionalized glycoporphyrins showed selectivity towards malign melanoma cells. We foresee that our findings will aid in the chemical design of porphyrin-based theranostic agents. The FDG-conjugated glycoporphyrins can also be evaluated as PET imaging agents, as well as for PDT in cancer and infectious diseases.

Experimental Section

Full experimental details including additional characterization data and NMR spectra of new compounds are given in the Supporting Information.

Acknowledgements

Our work is supported by the Swedish Foundation for Strategic Research (K.P.R.N, H.A.) and the Swedish Research Council (K.P.R.N., K.A., M.E.). We also thank Jörgen Adolfsson for technical support with the flow cytometry experiments.

Conflict of Interest

The authors declare no conflict of interest.

Keywords: cancer · glycoporphyrins · imaging · photodynamic therapy · photosensitizers

[1] R. Kojima, D. Aubel, M. Fussenegger, *Curr. Opin. Chem. Biol.* **2015**, *28*, 29 – 38.
[2] M. Ethirajan, Y. Chen, P. Joshi, R. K. Pandey, *Chem. Soc. Rev.* **2011**, *40*, 340 – 362.
[3] L. B. Josefsen, R. W. Boyle, *Theranostics* **2012**, *2*, 916 – 966.
[4] U. Chilakamarthi, L. Giribabu, *Chem. Rec.* **2017**, *17*, 775 – 802.
[5] P. Maillard, B. Loock, D. S. Grierson, I. Laville, J. Blais, F. Doz, L. Desjardins, D. Carrez, J. L. Guerquin-Kern, A. Croisy, *Photodiagn. Photodyn. Ther.* **2007**, *4*, 261 – 268.
[6] S. Vedachalam, B.-H. Choi, K. K. Pasunooti, K. M. Ching, K. Lee, H. S. Yoon, X.-W. Liu, *Med. Chem. Commun.* **2011**, *2*, 371 – 377.
[7] R. Daly, G. Vaz, A. M. Davies, M. O. Senge, E. M. Scanlan, *Chem. Eur. J.* **2012**, *18*, 14671 – 14679.
[8] S. Hirohara, Y. Kawasaki, R. Funasako, N. Yasui, M. Totani, H. Alitomo, J. Yuasa, T. Kawai, C. Oka, M. Kawaichi, M. Obata, M. Tanihara, *Bioconjugate Chem.* **2012**, *23*, 1881 – 1890.
[9] M. Tanaka, H. Kataoka, S. Yano, H. Ohi, K. Moriwaki, H. Akashi, T. Taguchi, N. Hayashi, S. Hamano, Y. Mori, E. Kubota, S. Tanida, T. Joh, *Mol. Cancer Ther.* **2014**, *13*, 767 – 775.
[10] M. Tamura, H. Matsui, S. Hirohara, K. Kakiuchi, M. Tanihara, N. Takahashi, K. Nakai, Y. Kanai, H. Watabe, J. Hatazawa, *Bioorg. Med. Chem.* **2014**, *22*, 2563 – 2570.
[11] J. Tang, J. J. Chen, J. Jing, J. Z. Chen, H. Lv, Y. Yu, P. Xu, J. L. Zhang, *Chem. Sci.* **2014**, *5*, 558 – 566.
[12] N. Hayashi, H. Kataoka, S. Yano, M. Tanaka, K. Moriwaki, H. Akashi, S. Suzuki, Y. Mori, E. Kubota, S. Tanida, S. Takahashi, T. Joh, *Mol. Cancer Ther.* **2015**, *14*, 452 – 460.
[13] X. S. Ke, Y. Ning, J. Tang, J. Y. Hu, H. Y. Yin, G. X. Wang, Z. S. Yang, J. Jie, K. Liu, Z. S. Meng, Z. Zhang, H. Su, C. Shu, J. L. Zhang, *Chemistry* **2016**, *22*, 9676 – 9686.
[14] O. Warburg, *Science* **1956**, *123*, 309 – 314.
[15] V. Ganapathy, M. Thangaraju, P. D. Prasad, *Pharmacol. Ther.* **2009**, *121*, 29 – 40.
[16] C. C. Barron, P. J. Bilan, T. Tsakiridis, E. Tsiani, *Metabolism.* **2016**, *65*, 124 – 139.
[17] J. Pacák, Z. Točík, M. Černý, *Chem. Commun.* **1969**, 77 – 77.
[18] J. Adamson, A. B. Foster, L. D. Hall, R. H. Hesse, *Chem. Commun.* **1969**, 309 – 310.
[19] T. Ido, C.-N. Wan, V. Casella, J. S. Fowler, A. P. Wolf, M. Reivich, D. E. Kuhl, *J. Labelled Compd. Radiopharm.* **1978**, *14*, 175 – 183.
[20] S. Vallabhajosula, L. Solnes, B. Vallabhajosula, *Semin. Nucl. Med.* **2011**, *41*, 246 – 264.
[21] G. Ribeiro Morais, R. A. Falconer, I. Santos, *Eur. J. Org. Chem.* **2013**, 1401 – 1414.
[22] G. T. Mukosera, T. P. Adams, R. F. Rothbarth, H. Langat, S. Akanda, R. G. Barkley, R. D. Dolewski, J. V. Ruppel, N. L. Snyder, *Tetrahedron Lett.* **2015**, *56*, 73 – 77.
[23] V. V. Rostovtsev, L. G. Green, V. V. Fokin, K. B. Sharpless, *Angew. Chem.* **2002**, *114*, 2708 – 2711.
[24] C. W. Tornøe, C. Christensen, M. Meldal, *J. Org. Chem.* **2002**, *67*, 3057 – 3064.
[25] M. A. Grin, I. S. Lonin, A. I. Makarov, A. A. Lakhina, F. V. Toukach, V. V. Kachala, A. V. Orlova, A. F. Mironov, *Mendeleev Commun.* **2008**, *18*, 135 – 137.
[26] J. S. Lindsey, *Acc. Chem. Res.* **2010**, *43*, 300 – 311.
[27] F. Li, K. Yang, J. S. Tyhonas, K. A. MacCrum, J. S. Lindsey, *Tetrahedron* **1997**, *53*, 12339 – 12360.
[28] A. P. Krapcho, G. A. Glynn, B. J. Grenon, *Tetrahedron Lett.* **1967**, *8*, 215 – 217.
[29] X.-A. Wu, P. Ying, J.-Y. Liu, H.-S. Shen, Y. Chen, L. He, *Synth. Commun.* **2009**, *39*, 3459 – 3470.
[30] J. Mason, S. Murphree, *Synlett* **2013**, *24*, 1391 – 1394.
[31] A. Y. Chernyak, G. V. M. Sharma, L. O. Kononov, P. R. Krishna, A. B. Levinsky, N. K. Kochetkov, A. V. Rama Rao, *Carbohydr. Res.* **1992**, *223*, 303 – 309.
[32] S. Nakabayashi, C. D. Warren, R. W. Jeanloz, *Carbohydr. Res.* **1986**, *150*, c7 – c10.
[33] T. Yohino, K. Sato, F. Wanme, I. Takai, Y. Ishido, *Glycoconjugate J.* **1992**, *9*, 287 – 291.
[34] M. Elgland, P. Nordeman, T. Fyrner, G. Antoni, K. P. R. Nilsson, P. Konradsson, *New J. Chem.* **2017**, *41*, 10231 – 10236.

[35] G. Garcia, D. Naud-Martin, D. Carrez, A. Croisy, P. Maillard, *Tetrahedron* **2011**, *67*, 4924 – 4932.
[36] B. Minaev, M. Lindgren, *Sensors* **2009**, *9*, 1937 – 1966.
[37] R. Vestberg, A. Nyström, M. Lindgren, E. Malmström, A. Hult, *Chem. Mater.* **2004**, *16*, 2794 – 2804.
[38] E. Glimsdal, I. Dragland, M. Carlsson, B. Eliasson, T. B. Melø, M. Lindgren, *J. Phys. Chem. A* **2009**, *113*, 3311 – 3320.
[39] J. W. Snyder, E. Skovsen, J. D. C. Lambert, L. Poulsen, P. R. Ogilby, *Phys. Chem. Chem. Phys.* **2006**, *8*, 4280 – 4293.
[40] P. R. Ogilby, *Chem. Soc. Rev.* **2010**, *39*, 3181 – 3229.

Received: February 9, 2018
Version of record online May 18, 2018

